DOI: 10.1021/ma102152j

Macromolecules
ARTICLE

Study of Water Adsorption in Poly(*N*-isopropylacrylamide) Thin Films Using Fluorescence Emission of 3-Hydroxyflavone Probes

Cheryl Morris,[†] Boguslaw Szczupak,[†] Andrey S. Klymchenko,[‡] and Alan G. Ryder*,[†]

[†]*Nanoscale Biophotonics Laboratory, School of Chemistry, National University of Ireland, Galway, Galway, Ireland, and* [‡]*Laboratoire de Biophotonique et Pharmacologie, UMR 7213 CNRS, Université de Strasbourg, Faculté de Pharmacie, 74, Route du Rhin, 67401 ILLKIRCH Cedex, France*

Received September 16, 2010; Revised Manuscript Received October 11, 2010

ABSTRACT: The noncontact measurement of water uptake in microscale (1−100 μm), thermoresponsive poly(*N*-isopropylacrylamide) thin films is challenging. We assessed the efficacy of three different 3-hydroxyflavone (3-HF)-based fluorophores to monitor water uptake in pNIPAM thin films close to the lower critical solution temperature (LCST) at 25 and 37 °C. These 3-HF fluorophores undergo excited-state intramolecular proton transfer, yielding emission from normal (N*) and tautomeric (T*) excited-state forms. The emission intensity ratio, $\log(I_{N^*}/I_{T^*})$, and N* band position are environmentally sensitive. Water adsorption in pNIPAM thin films follows a nonlinear, two-phase process: at low relative humidity, the adsorbed water disrupts polymer−fluorophore hydrogen bonding, yielding small changes in $\log(I_{N^*}/I_{T^*})$ ratios and overall intensity; at higher relative humidity, these intensity parameters (but not fluorescence lifetime) change dramatically, indicating a larger change in local polarity. These probes are thus sensitive indicators of water uptake in pNIPAM.

Introduction

Within biomedical science and engineering the use of microscale (< 100 μm) thin polymer films is widespread, with roles in tissue engineering, drug delivery systems, microfluidic devices, bioadhesion mediators, and bioactuators.[1−14] One potential use is as coatings on drug eluting coronary stents, where the polymer can act both as a drug reservoir (e.g., providing local antirestenosis therapy) and as a biocompatibility modulator to improve device performance.[4,5,15,16] Thus, the choice of polymer for such applications is very important, as coating stability, device efficacy, long-term storage, and other parameters are all dependent on the physiochemical properties of the polymer.[17] One area of significant interest recently has been the development of synthetic functional polymers that display stimuli or environmental responsive behavior, with the intention of providing "smart" applications in the biomedical field.[1,18,19] Stimuli responsive polymers can be defined as polymers that undergo a nonlinear response due to the application of an external environmental stimulus such as ionic strength, light, pH, temperature, etc.[10,11,18−23]

Thermoresponsive polymers are probably the most widely studied stimuli responsive polymers and, as the name suggests, undergo conformational changes in response to temperature. Thermoresponsive systems display a critical solution temperature, at which a phase change of the polymer solution occurs in accordance with the polymer composition.[20] In some cases, due to enthalpic effects, polymer systems can become more solvated with increasing temperature; however, in contrast, the thermal responsiveness of certain polymer systems is based on the existence of a lower critical solution temperature (LCST).[24,25] Solutions of polymers exhibiting a LCST appear biphasic above and monophasic below a certain temperature.[20] Thus, these polymers become less solvated on increasing temperature, leading to the eventual precipitation of the polymer from solution at the LCST.[24] These types of polymers generally have a wide variety of potential applications from cell culture to local drug delivery.[26]

*Corresponding author. E-mail: alan.ryder@nuigalway.ie.

Poly(*N*-substituted acrylamides) are a family of thermoresponsive polymers displaying a LCST, and poly(*N*-isopropylacrylamide) (pNIPAM) is probably the most widely studied.[27] In aqueous solution, pNIPAM has a LCST at 32 °C; at this temperature it undergoes a sharp and reversible coil-to-globule phase transition from a hydrophilic to a more hydrophobic state, forcing water from the matrix.[2,5,9,19,22,28−30] This phenomenon occurs due to the domination of entropic effects (displacement of water from the polymer matrix) over enthalpic effects (formation of hydrogen bonds between polymer and water molecules) as the temperature increases above the LCST.[20,31] Below the LCST, pNIPAM chains exist in an extended coil conformation, and solvation is driven by the enthalpic gain from intermolecular hydrogen bonding between the pNIPAM chains and water molecules.[19,25] As the temperature is increased towards the LCST, pNIPAM chains undergo a coil-to-globule transition.[19] Intramolecular hydrogen bonding between carboxyl and amide groups on the pNIPAM chains results in the interruption of hydrogen bonding of these groups with water molecules, ultimately resulting in chains adopting a collapsed conformation, driving out the water, and causing the polymer to precipitate out of solution.[25] pNIPAM and its copolymers have displayed interesting qualities in pharmaceutical and biomedical applications due to their dramatic response to small changes in temperature.[6,8]

Water uptake in a supported polymer film can lead to significant changes in the physicochemical properties of the polymer, which in turn will affect mechanical properties, and this may lead, in medical devices, to such problems as reduced adhesion and mechanical properties, pronounced physical and chemical aging, and swelling and expansion, compromising the intended function of the polymer and also hindering biocompatibility.[32−36] In relatively hydrophilic polymers like pNIPAM, there is always likely to be an appreciable amount of water infiltrating the polymer if it is handled under ambient conditions and precautions are not taken to exclude water infiltration. The situation will be exacerbated when using thin films as the surface area is much larger and this will facilitate water uptake.

 Published on Web 10/27/2010 © 2010 American Chemical Society

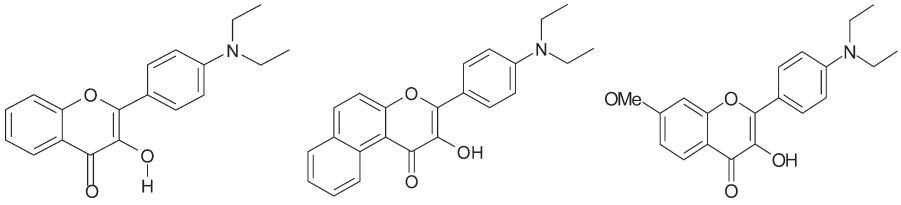

Figure 1. Chemical structures of the flavone-based probes 4-(diethylamino)-3-hydroxyflavone (FE), 5,6-benzo-4′-(diethylamino)-3-hydroxyflavone (BFE), and 4-(diethylamino)-3-hydroxy-7-methoxyflavone (MFE).

Methods of analysis for supported biomedical polymer films generally involve the analysis of two distinct domains: the surface of the polymer film or the bulk film. One of the most widely used characterization methods for thin films employed in biomedical applications is the contact angle method which is typically used to indicate changes in the hydrophobic−hydrophilic character and to estimate surface energy.[37,38] However, implementing the contact angle method on hydrophilic polymer systems where appreciable water adsorption occurs under normal conditions is problematic, and the results are subjective at best. Water infiltration into thin films can be significant, and one would expect that this could induce changes in the physicochemical properties.

Thus, there is a need for a noncontact, nondestructive method of polymer characterization for supported films that can show the changes induced by adsorption of water under normal environmental conditions. The degree and rate of water uptake will be largely governed by the polymer composition, and less dense polymers incorporating polar groups that can hydrogen bond strongly with the incoming water will obviously adsorb greater quantities of water. The changes in polarity induced by the adsorbed water can be sensed using UV−vis absorption spectroscopy[17] or by fluorescence spectroscopy if the probes are sensitive to polarity and/or hydrogen-bonding effects.[39,40] Fluorescence spectroscopy is a powerful tool for monitoring microscopic changes in polymer systems due to the high sensitivity and selectivity, short response time, and nondestructive nature of the measurement.[41] However, in the case of fluorophores with a single emission band, there are problems such as photobleaching, excitation source instabilities, and variations in probe concentration which can make measurements unreliable, particularly in viscous/rigid polymers.[32−35] One means of overcoming such problems would be through the use of ratiometric fluorophores. One such class of ratiometric fluorophores are the 3-hydroxyflavones.[42,43]

Derivatives of 3-hydroxyflavone undergo excited-state intramolecular proton transfer (ESIPT) and exhibit two emission bands: from the normal excited state (N*) and the other from the ESIPT reaction product phototautomer (T*). Both forms are highly emissive, and their spectral bands are well separated on the wavelength scale.[44,45] ESIPT involves an intramolecular transfer of a hydroxyl proton to a carbonyl oxygen via the H-bond.[44] Absorption of a photon of light generates the normal Franck−Condon excited state which then relaxes to the N* state. The N* state can then undergo ESIPT to the T* state followed by emission of a photon of light results in the population of the ground T state with proton back-transfer to the N state.[45] It is important that the four states N, T, N*, and T* possess different distribution of charges and interact differently with the environment. Because of significant differences between the N* and T* states, the intensities of the emission from the two states (I_{N^*} and I_{T^*}) can be considered as independent variables. The ratio of intensities of these two states, I_{N^*}/I_{T^*}, is an important parameter which is connected to the relative energies of the N* and T* states and is a sensitive indicator of polarity.[45] Use of such fluorophores allows the determination of a set of parameters which can differently characterize the physical properties of the microenvironment. The spectroscopic behavior of the N* and T* bands depends strongly on the structure of the specific fluorophore, and structural modifications can modulate sensitivity to H-bonding and solvent polarity.[46−48]

Three derivatives of 3-hydroxyflavone were used in this study: 4′-(diethylamino)-3 hydroxyflavone (FE), 5,6-benzo-4′-(diethylamino)-3-hydroxyflavone (BFE), and 4′-(diethylamino)-3-hydroxy-7-methoxyflavone (MFE) (Figure 1). These probes in solvent environments with increasing polarity show an increase of the N* form relative to the T* form.[45,47,48] The log ratio of the emission intensities of the N* and T* forms $\log(I_N^*/I_T^*)$,[45] has been shown to be linearly correlated with polarity for solvents.[45,47,48] However, the polymer case is more complex, and we have previously shown that while these 3-HF probes can be used to measure changes in the chemical composition of dry, random-linear, hydrophilic/hydrophobic thermoresponsive copolymer films, they cannot be used for quantitative polarity measurements using simple emission parameters such as $\log(I_N^*/I_T^*)$. This is because of heterogeneity in the ground state hydrogen bonding, which is evidenced by excitation wavelength dependence and the time-resolved fluorescence data obtained for the N* and T* band emission.[40,49,50]

In medical device manufacturing where thin polymer films are widely used, the ability to observe water adsorption and understand its subtle characteristics will be important for the development of robust manufacturing practices. Here we study water uptake in pNIPAM thin films supported on quartz surfaces by studying the fluorescence emission properties of a series of 3-HF fluorophores to determine which probe offers the best sensitivity to water uptake and to study in detail the dynamic hydration processes in thin film hydrophilic polymers. In particular, the high sensitivity of this fluorescence method enables one to observe the subtle changes that occur with low amounts of adsorbed water.

Experimental Section

Materials. Poly(*N*-isopropylacrylamide) (pNIPAM) with an average molecular weight of 20 000−25 000 was purchased from Sigma-Aldrich and used as received. The pNIPAM was stored without taking any particular precautions (e.g., controlling humidity) at room temperature. The fluorescence probes 4′-(diethylamino)-3-hydroxyflavone (FE), 5,6-benzo-4′-(diethylamino)-3-hydroxyflavone (BFE), and 4-(diethylamino)-3-hydroxy-7-methoxyflavone (MFE) were synthesized as previously described, and their structures are shown in Figure 1.[45,47,48] All the steady-state fluorescence measurements reported were made over a period of 3 months using a single 10 g batch of the pNIPAM polymer. The lifetime data were collected on the same batch of polymer ∼5 months later.

Thin Film Preparation. Quartz slides of dimensions 12 mm × 45 mm × 1.5 mm (from Lightpath Optical Ltd. UK) were used as the supporting substrates for the polymer films. Prior to film casting, the quartz slides were washed at least three times with acetone, methanol, and deionized water and were dried in an oven at 70 °C. The films were cast onto the quartz slides yielding dry films of 10 μm in thickness (measured using a micrometer gauge) using the following procedure. 5.4 mg of the solid polymer was dissolved in 137.5 μL of a 5.7×10^{-5} M ethanol solution of the requisite probe (∼5 wt % solution). The solution was then carefully spread onto the quartz

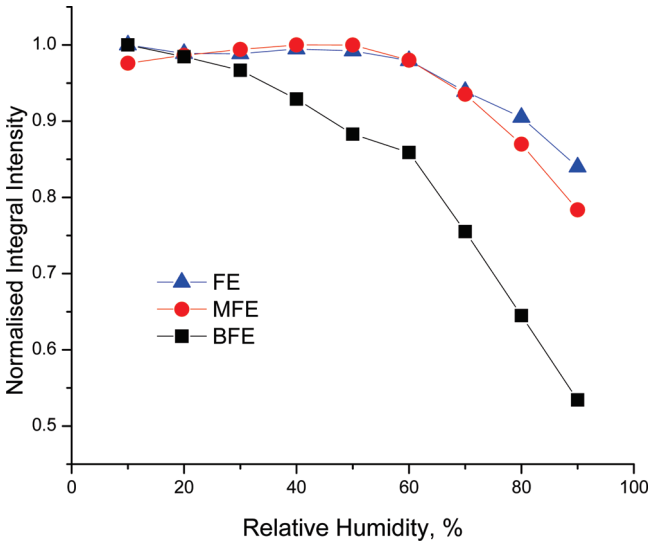

Figure 2. Plot of normalized integral intensity vs relative humidity for thin pNIPAM films doped with FE, BFE, and MFE.

substrate and cured for 24 h in a sealed ethanol environment. The ethanol was present to saturate the atmosphere above the polymer film to prevent water infiltration into the films during the curing process. On removal of the films from the ethanol environment they were placed in an oven at 70 °C for 48 h to complete the drying process. By visual inspection, the films obtained were smooth, transparent, and free of any inhomogeneities. For the reproducibility measurements (Figure 2) a 5 wt % pNIPAM solution was used to generate the thin films.

Instrumentation. A VGI2000 M controlled humidity chamber (Surface Measurement Systems Ltd. UK) was used to generate a precisely controlled humidity and temperature environment in which the thin films were placed. A precise humidity level is generated within the chamber by mixing water saturated nitrogen (N_2) gas with dry N_2 gas in the appropriate proportion under computer control. In general, all tests began at 10% relative humidity (RH), and then the relative humidity was increased in 10% increments at hourly intervals. The hour interval between measurements was the minimum required to allow for equilibration of water content between the chamber and polymer. After the final measurement at 90% RH was made, the sample was then removed and dried at 70 °C for 84 h before making any replicate measurements. This minimum drying time was established by trial and error experimentation. This long drying time was required to completely remove water from the polymer matrix because if any residual water were present, it adversely affected measurement reproducibility. Each sample was analyzed in triplicate at 25 and 37 °C (above and below pNIPAM LCST).

Spectroscopic Measurements. Spectral data (time-resolved and steady-state) were collected via the transparent glass window of the humidity chamber. For steady-state fluorescence emission measurements the excitation source was a fiber coupled modulated 405 nm laser diode (MDL300, PicoQuant), and the detection system was a fiber optic coupled miniature spectrometer (USB2000, Ocean Optics). The excitation and emission fibers were coupled into a home-built assembly which has a dichroic beamsplitter to reflect the excitation light down into the chamber and then pass the emission upward, through a 430 nm cutoff emission filter into a 1000 μm diameter optical fiber connected to the USB spectrometer. The resulting steady-state spectra were not corrected for instrument response (see Supporting Information) which can be significant due to polarization and optical effects. Thus, caution should be exercised when comparing these steady-state emission spectra with other published data; however, for the purposes of this discussion with regard to the relative changes due to humidity and probe structure we do not require the use of corrected spectra. The $\log(I_{N*}/I_{T*})$ ratios and full width at half-maximum (fwhm) values were calculated by using a two-band Gaussian fit (in Origin ver. 7.0, OriginLab Corporation, Northampton, MA) to the uncorrected spectra. For band fitting, the spectra were first smoothed (using the FFT function) and then baseline corrected. The normalized integral intensity was calculated, again using Origin 7, by means of the calculus-integrate function (integration was performed over the 425−600 nm spectral range).

For the fluorescence lifetime measurements a fiber-optic reflection probe (R400-7, UV−vis, Ocean Optics) with one illumination and six read fibers (all 400 μm diameter) was used to couple the excitation light into and the fluorescence emission out of the chamber. A pulsed 405 nm laser diode (PicoQuant) was used as the excitation source, and this was coupled into the central fiber of the optical probe. The fluorescence emission collected by the probe was coupled via a wedge depolarizer (WDPOL, Thorlabs) into an in-house assembled time-correlated single photon counting (TCSPC) system. This comprised of a monochromator (model 9030, Sciencetech, Canada) with a photon counting PMT detector (model H5783, Hamamatsu). Data collection was controlled by a PicoHarp 300 TCSPC system (PicoQuant). The instrument response function (IRF) was generated by collecting the scattered laser light from a clean quartz slide target which was placed inside the humidity chamber. Lifetimes were measured at emission wavelengths of 489 nm (N* maximum) and 564 nm (T* maximum) for FE, 487 and 567 nm for MFE, and at 502 and 563 nm for BFE. In each case, data were collected until there were 10 000 counts in the channel of maximum intensity, and then fluorescence lifetimes were extracted from the measured decay curves using FluoFit (ver. 4.2, PicoQuant) which implements nonlinear least-squares error minimization analysis, based on the Simplex and Levenberg−Marquardt algorithms. The final quoted result was determined by the fit, which had a χ^2 value of less than 1.2 and a residual trace that was symmetric about zero (see Supporting Information for detailed fits of the lifetime data). The fiber-optic-based sampling arrangements yielded a sample spot size of ~5 mm^2 for all the spectroscopic measurements undertaken.

Water Uptake Mass Measurements. The pNIPAM thin films have a very significant water absorption capacity at 25 °C (below LCST) and at 37 °C (above LCST) as measured using the following simple procedure. A dry thin film sample was taken from an oven and weighed immediately using a microbalance. The sample was then placed in the humidity chamber at 25 °C (or 37 °C) and 90% relative humidity (RH) for ~6 h. The sample was then removed from the chamber and weighed immediately. The difference in weight between the "dry" and "wet" weights was taken to be the mass uptake of water by the sample. For a 10 μm thick pNIPAM film with a dry weight of 4.9 mg, at 25 °C and 90% RH, 1.3 mg (26.5 wt %) of water was absorbed. For a similar 10 μm thick pNIPAM film with a dry weight of 4.9 mg, at 37 °C and 90% RH, we found that 0.3 mg (6.1 wt %) of water was absorbed.

Results and Discussion

The first critical point in the measurement of emission data using the humidity chamber was to understand the dynamics of the equilibration of water between the chamber environment and the polymer thin film. Initial measurements were made using short equilibration times of 10−15 min between changes in humidity level. These fluorescence measurements showed considerable hysteresis in the plot of $\log(I_{N*}/I_{T*})$ vs RH (Supporting Information) when the humidity was cycled from low (10% RH) to high (90% RH) and back to low (10% RH). Reproducibility was found to be extremely dependent on the equilibration time at each step where a change in the relative humidity was made and also on film drying prior to placement in the chamber. The equilibration time is obviously a function of polymer composition and water content level, and we found that for thin pNIPAM films a minimum 1 hour equilibration period was required for

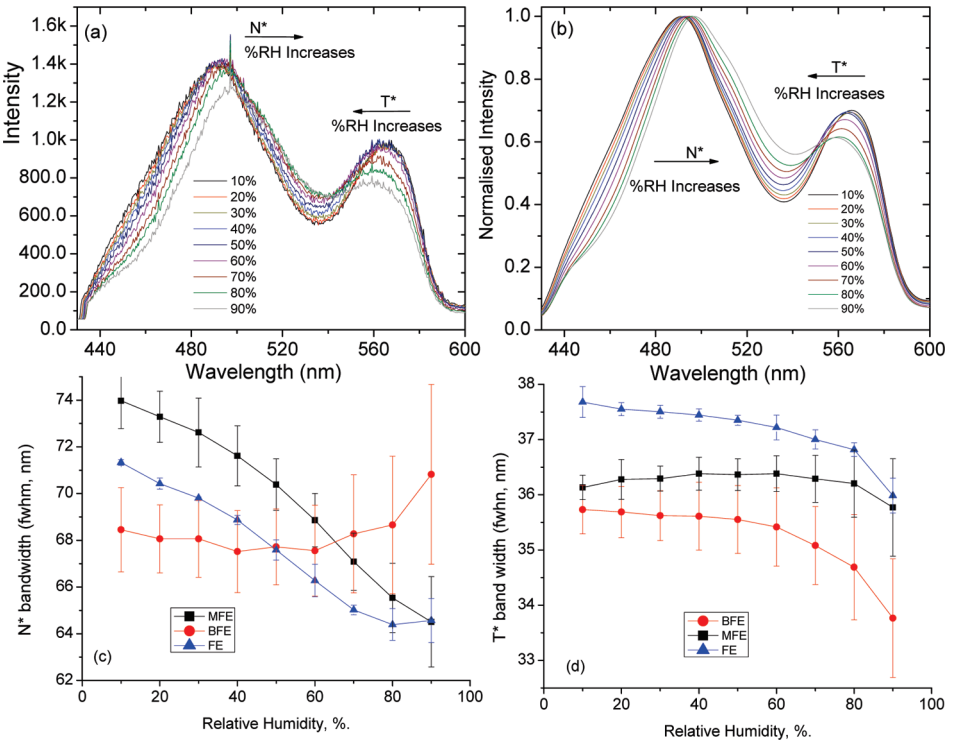

Figure 3. (a) Raw fluorescence emission spectra of FE (uncorrected for instrument response) collected at different relative humidity (between 10% and 90%). With increasing humidity the N* band is red-shifted (~10 nm) while the T* band is blue-shifted (~2 nm). (b) Normalized, smoothed spectra of same. The distortion in the emission spectra visible below ~450 nm is due to the cutoff filter used to eliminate scattered excitation light. (c) Plot of N* bandwidths (full widths at half-maximum, nm) for all three probes vs increasing humidity. (d) Plot of T* bandwidths (fwhm, nm) for all three probes vs increasing humidity. The fwhm values were calculated by software decomposition of the spectra to two Gaussian functions.

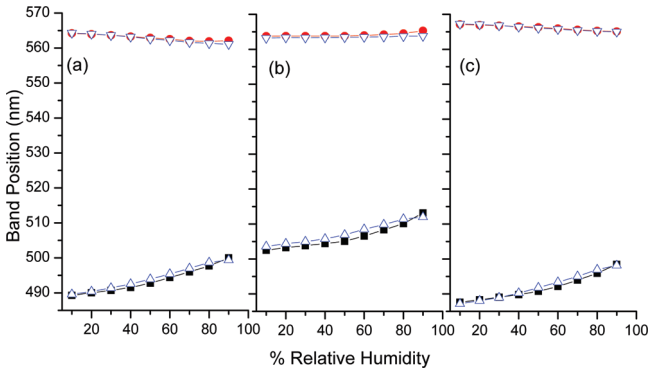

Figure 4. Plot of variation in N* and T* band positions against increasing %RH (■, N* band position at 25 °C; ●, T* band position at 25 °C; △, N* band position at 37 °C; ▽, T * band position at 37 °C) for pNIPAM doped with (a) FE, (b) BFE, and (c) MFE.

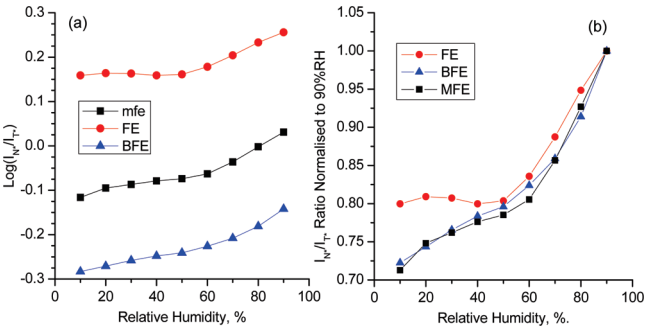

Figure 5. (a) Plot of the $\log(I_{N^*}/I_{T^*})$ ratio vs increasing relative humidity at 25 °C for pNIPAM films doped with BFE (▲), MFE (■), and FE (○). (b) Plot of the I_{N^*}/I_{T^*} ratio normalized to the value recorded at 90% RH.

every 10% change in RH. We also noted from replicate measurements that the standard deviation in the measurements is larger at the lower RH, and this might be expected as one would expect the dry polymers to have a significant water uptake capacity. Thus, at low RH, the amount of available water present is low, so it will take longer to extract sufficient water out of the environment and diffuse throughout the polymer and establish an equilibrium.

At 25 °C (below the LCST), as the humidity increases and water is absorbed by the pNIPAM film, the overall fluorescence emission intensity decreases (Figure 2), there is a wavelength shift for both emission bands (Figures 3 and 4), and the emission intensity ratio (I_{N^*}/I_{T^*}) changes (Figure 5). For FE and MFE the overall intensity change seems to follow two distinct phases: first, a small increase in intensity up to ~50% RH, followed by a much steeper decrease at higher water concentrations. For BFE, the intensity changes are more pronounced, and we see a large decrease at low humidity followed by a much steeper decrease above ~60% RH. This intensity decrease at higher RH is probably due to water induced static quenching.

The emission of these probes also provides information about changes in the microheterogeneity of the polymer matrix, with wider bands indicating a greater degree of heterogeneity. The change in intensity at the maximum of the N* and T* bands is also accompanied by significant changes in the full width at half-maximum (fwhm) of the emission bands (Figure 3c,d), and again we see dramatic differences between FE/MFE on one hand and BFE on the other. For the N* band of FE and MFE, as humidity increases there is a decrease in bandwidth (fwhm) of ~10 nm, indicating that the fluorophores are now experiencing a narrower range of microenvironments as water is absorbed (Figure 3c). For BFE, the situation is reversed, and at the higher relative humidity (> 60%) the bandwidth increases slightly (by ~3 nm), indicating that the N* state is experiencing a slightly more heterogeneous environment. In contrast, the T* bandwidth seems to decrease

Table 1. Fluorescence Lifetime Data vs Increasing Relative Humidity at 25°C for pNIPAM Films Doped with FE[a]

rel humidity (%)	band	τ_1 (ns)	τ_2 (ns)	τ_3 (ns)	α_1	α_2	α_3	τ_{AV} (ns)	χ^2
10	N*	0.25	1.35	2.51	0.23	0.25	0.52	2.22	0.99
10	T*	0.13	2.19	3.48	−0.29	0.29	0.42	3.14	1.06
30	N*	0.25	1.21	2.53	0.21	0.23	0.56	2.25	1.02
30	T*	0.12	2.44	3.66	−0.29	0.4	0.3	3.13	1.05
50	N*	0.32	1.26	2.54	0.20	0.23	0.57	2.26	0.96
50	T*	0.20	2.52	3.84	−0.19	0.56	0.25	3.09	1.05
70	N*	0.26	1.20	2.56	0.24	0.22	0.54	2.27	0.96
70	T*	0.23	2.48	3.64	−0.27	0.5	0.24	3.03	0.99
90	N*	0.24	1.16	2.57	0.25	0.22	0.53	2.27	0.99
90	T*	0.34	2.22	3.22	−0.22	0.35	0.44	2.95	1.12

[a] All data fitted to a triexponential model. N* data measured at 490 nm; T* data measured at 590 nm. The full fit data for BFE and MFE are provided in the Supporting Information. τ_{AV} = intensity averaged lifetime, α_i = fractional amplitudes/pre-exponential factors. Amplitudes normalized such that $\sum|\alpha_i| = 1$.

slowly (~1.5 nm) for FE and MFE at relative humidity below ~80% but then decreases more rapidly above ~80% RH. For BFE, there is a slightly larger decrease of ~3 nm at higher relative humidity, above ~50% RH, which may indicate a more homogeneous T* environment. The greater error in the BFE measurements is due to difficulties in getting reproducible, replicate measurements, which arose largely from the much greater photobleaching encountered with this fluorophore (see Supporting Information).

As humidity increases, the N* band emission is red-shifted by up to 10 nm (and the change can be fitted to a quadratic function) while the T* band emission is blue-shifted by a much smaller amount (~2 nm) and the same trend was observed for each of the three fluorophores (Figure 4). These systematic changes which lead to a decrease in the N* and T* band separation have been observed only in protic solvents.[45] As was shown previously, the significant polymer−probe hydrogen bonding in these polymers accounts for the large N*−T* band separation.[49] As with the intensity changes, there are two stages of wavelength shifts: first, a small change (< 2 nm) below ~40% RH and then a more dramatic variation at higher water content. This indicates that the degree of N* state dielectric stabilization is greater when there is more water present.

Plotting the log of intensity ratio ($\log(I_{N*}/I_{T*})$) vs % RH for all three fluorophores (Figure 5a), it is apparent that with increasing humidity $\log(I_{N*}/I_{T*})$ also increases but at two different rates, with the greatest increase occurring at the higher relative humidity's above ~50% RH. This occurs because of the dramatic increase in micropolarity due to water absorption, which in turn causes a greater relative dielectric stabilization of the N* state compared to the T* state and leads to an increase in the intensity of the N* emission relative to the T* emission.[45] It is easier to observe the magnitude of the water-induced changes by comparing the normalized values of the I_{N*}/I_{T*} ratios (using the 90% RH value as the denominator, Figure 5b). We note that both BFE and MFE have the largest relative changes whereas there is virtually no significant change for FE at the lower water adsorption content. The significantly larger changes in $\log(I_{N*}/I_{T*})$ as a function of humidity for MFE, coupled with its relatively good photostability, makes it the best probe for studying water uptake dynamics in these thin polymer films.

To understand in more detail the photophysics, fluorescence lifetime data were collected for all probes under conditions of varying humidity. For both N* and T* bands the decays were multiexponential. We observed very little or no change in average lifetime or the component lifetimes for each band with increasing humidity (Table 1 and Supporting Information). For FE, the fractional amplitudes do not vary much in the relative humidity range sampled. Normally, FE derivatives in organic solvents present two decay times for both N* and T* bands. Moreover, due to reversible ESIPT reaction of FE in organic solvents, the following observations were reported:[51] (i) a short decay time for the N* band corresponding to the ESIPT reaction, whereas for the T* band, the same decay time is associated with a negative pre-exponential component; (ii) the long lifetimes associated with N* and T* bands are the same; and (iii) the pre-exponential coefficients for the T* band emission decay are opposite in sign and of the same magnitude.[51] In the present polymer study, we also found similar features in the time-resolved data. Indeed, the short- and long-lived components of the N* and T* bands are rather close, while the pre-exponential coefficients of the T* emission are opposite in sign and similar in amplitude. Thus, we could speculate that FE probe and its analogues may undergo reversible ESIPT reaction in the polymer. However, the observed additional third component for the N* emission of the probes in the polymer may suggest the presence of H-bonded probe−polymer complexes with different ability to undergo ESIPT. There are two possible H-bond interactions between the polymer and the FE and MFE probes that will strongly influence the ESIPT process. The first interaction being between the 4-carbonyl group of the probes and the amide hydrogen of the polymer was previously reported to decrease significantly the ESIPT rates.[52] In contrast, the second type of complex featuring H-bonding between the 3-hydroxy group of the probes and the carbonyl group of the polymer should disrupt the intramolecular H-bonding and, thus, the ESIPT process. The presence of these two different complexes could explain the additional decay time, which was not observed in aprotic organic solvents.[51] Thus, the FE probe and its analogues in polymers present at least two populations: one undergoing reversible ESIPT, while the other being strongly bound with an inhibited ESIPT process (lifetime around 1.2 ns of N* band). This is consistent with what was previously observed for a different pNIPAM polymer and NIPAM−NtBA copolymers.[49,50] Finally, the weak sensitivity of the time-resolved data to humidity changes indicates that the observed fluorescence quenching at higher humidity (Figure 2) is static in nature, and therefore one can conclude that the water is strongly bound to the polymer and not present in a freely diffusing manner.

It is clear that these 3-HF probes sense two distinct physicochemical environments as the humidity increases and more water is absorbed by the polymer film. All the observed data can be explained by variations in hydrogen-bonding interactions, and we had previously observed this interaction in pNIPAM and NIPAM−NtBA copolymers.[49] However, it is obvious that pNIPAM under these water uptake conditions is a relatively strong protic environment, based on solvatochromic measurements[17] which showed that pNIPAM was a strong hydrogen bond acceptor ($\beta = \sim 0.76 \pm 0.03$) and a moderately strong hydrogen bond donor ($\alpha = \sim 0.40 \pm 0.03$). The FE probe has an extremely low quantum yield in water (< 0.3%) but a relatively high quantum yield in protic solvents which are strong H-bond acids. Therefore, the absence of the quenching of the dyes at low humidity is probably because the water molecules are strongly associated with the polymer.

In this "relatively dry" domain, the incoming water will preferentially locate in the hydrophilic polymer domains where the most polar groups of the polymer are located. It is our contention that this incoming water first hydrogen bonds strongly to the polymer N−H and C═O groups and therefore does not solvate the probe. This is supported by molecular dynamics studies of water interactions in pNIPAM by Tamai[53,54] which indicates that water molecules are strongly bound to the −NH and the C═O of the polymer at relatively low water content. Thus, the $\log(I_{N*}/I_{T*})$ value for FE (Figure 5) is relatively constant at these lower water levels because this polymer-bound water does not have a very significant impact on the ESIPT process. In the case of MFE, the weak methoxy electron donor at the 7-position decreases the charge transfer character of the N* state of the dye, making the N* state dielectrically less stabilized, which favors the ESIPT product,

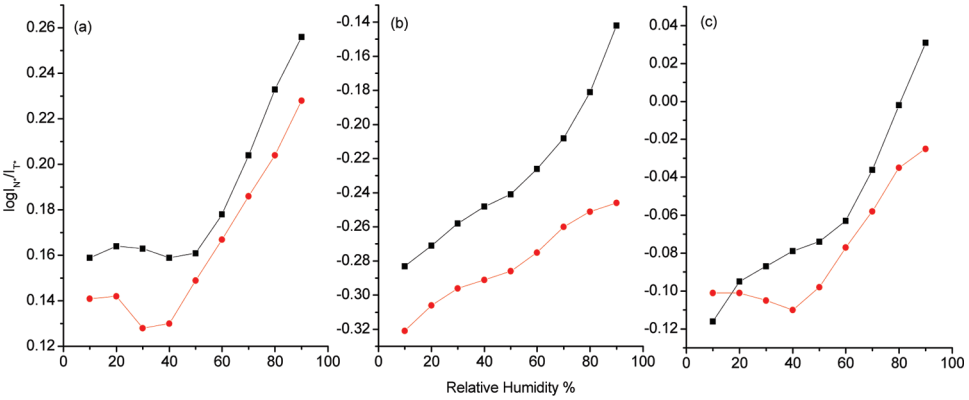

Figure 6. Plot of the log(I_{N*}/I_{T*}) ratio vs increasing humidity of pNIPAM films doped with (a) FE, (b) BFE, and (c) MFE at 25 °C (■) and 37 °C (●).

T* state, giving a lower log(I_{N*}/I_{T*}) ratio at all humidity values (Figure 5a). In contrast to FE and MFE, BFE should be less sensitive to hydrogen bonding with 4-carbonyl because of its steric hindrance by the additional benzyl group;[47] nevertheless, BFE is more sensitive to humidity changes than FE and in fact has an almost identical to relative sensitivity to MFE (Figure 5b). This suggests that it is the specific interaction between the 3-OH of the probe and the carbonyl group of the polymer (driven by the strong H-bond acceptor ability of pNIPAM[17]) which could be responsible for the observed probe response at low humidity. An alternative explanation could be that the humidity mainly affects the polarity of the polymer environment, but not its H-bond donor ability, which is in line with the observed red shifts of the N* emission bands for all the dyes on addition of water at low humidity (Figure 4). Thus, the additional water molecules are probably strongly H-bonded to the carbonyl oxygen of pNIPAM, which neutralizes the high H-bond donor ability of water and explains the absence of the specific H-bonding effects with FE and MFE dyes.

In the second phase hydration, where there is a greater adsorbed water content (> 50% RH), the incoming water seems to preferentially associate with the water bound to the polymer (the primary hydration shell), generating larger "loosely bound" water domains within the polymer. The amount of adsorbed water is potentially considerable, since at 90% RH and at a temperature of 20 °C, bulk pNIPAM is capable of adsorbing a maximum of ~8% of its own weight in water.[55] Now for all of the probes, we see dramatic changes in the log(I_{N*}/I_{T*}) ratio (Figure 5a), greater red shift of the N* band (Figure 4), decreases in fluorescence intensity (Figure 2), but no significant change in local heterogeneity experienced by the excited states (Figure 3c) (fwhm decreases for N* state, indicating a reduction in heterogeneity of the emitting states). So this second phase hydration produces spectral effects similar to those produced by the common solvent polarity effect with increasing dielectric stabilization of the N* state, causing a greater red shift of the N* band and a large relative increase in the log(I_{N*}/I_{T*}) ratio.[44] These effects are, however, very different from those obtained from the hydration of AOT reverse micelles.[44] In the hydration of the AOT micelles, the addition of water results in an increased ordering of the AOT molecules and the redistribution of the FE probe molecules into the apolar hexane phase, resulting in the log(I_{N*}/I_{T*}) ratio decrease. This does not happen in these polymers because there is no distinct apolar phase and there is no clear evidence for redistribution into more hydrophilic microdomains.

Above the LCST (32 °C) pNIPAM exists in a more hydrophobic, condensed state, and as such, the rate of water adsorption should be decreased. Previous reports using thermal gravimetric measurements on pNIPAM[55] indicated that no water was adsorbed at 40 °C (or, more correctly, it was not possible to measure the low amount of adsorbed water). However, this is not the case with thin films of this pNIPAM polymer at 37 °C, where we found absorption of at least 6 wt % of water using a simple mass measurement method. Furthermore, fluorescence analysis of the pNIPAM thin films show clearly that in every case the log(I_{N*}/I_{T*}) value increases with increasing humidity (Figure 6). This provides a noncontact indication that water has infiltrated the polymer above the LCST, interrupting the polymer−probe interaction. This is not surprising since the much larger surface area of the thin film will encourage adsorption compared to the bulk sample used in the reference.[55] The log(I_{N*}/I_{T*}) values for the 37 °C measurements are in all cases lower than the 25 °C measurements, which clearly indicates the less polar environment for the condensed polymer state above LCST. As water infiltrates the polymer, the polymer−probe interactions are supplanted by (polymer−water)−probe interactions, leading to an increasing stabilization of the N* state relative to the T* state, and we observe similar dependence of log(I_{N*}/I_{T*}) vs humidity to that observed at 25 °C. This indicates that in thin, micrometer scale films water adsorption will still be a significant issue above the LCST and that we can use these 3-HF probes to monitor this water infiltration.

Conclusions

We have shown that using a controlled humidity chamber one can easily study water uptake in thin thermoresponsive polymer films by measuring the fluorescence emission of 3-hydroxyflavone derivatives FE, MFE, and BFE. These dual band ratiometric probes were selected because their emission properties are sensitive to local polarity and hydrogen-bonding effects. Furthermore, the fact that there are multiple parameters available (intensity, emission bandwidth, band separation, band ratio, and lifetimes), one can obtain a more comprehensive picture of how water affects the polymer microenvironment than is possible with single band probes. The water adsorption process in thin pNIPAM films appears to follow two distinct phases. First at low relative humidity, the adsorbed water forms a primary hydration layer where all water molecules are strongly bound to the polymer and, therefore, do not produce a very strong spectroscopic effect on the probes. Moreover, the local microheterogeneity is maintained as one does not observe very significant changes in the emission bandwidth. At higher water content (relative humidity above 60%) the rate of change in log(I_{N*}/I_{T*}), fluorescence intensity, N* bandwidth, and band shifts increases dramatically, which indicates that the secondary hydration of the polymer now causes a larger change in local polarity and H-bonding interactions of the probe with water. This combination of effects has a much larger effect on the overall ESIPT process and thus the greater changes in emission parameters. The log(I_{N*}/I_{T*}) value for all three fluorophores increases, with BFE and MFE showing the greater sensitivity to increasing humidity compared to FE.

However, because BFE is strongly photobleached, we conclude that MFE is the best probe for assessing water ingress. When emission measurements were made above the LCST (37 °C), it was clear that the hydrophobic pNIPAM film was still absorbing some water because we could observe similar changes in the $\log(I_{N^*}/I_{T^*})$ values against increasing humidity. However, the magnitude of the $\log(I_{N^*}/I_{T^*})$ values were reduced in each case, which indicates that the local polarity is much less than that for measurements made below the LCST.

The use of the MFE dual band ratiometric probe in combination with a controlled humidity chamber offers considerable promise for studying in detail the hydration processes in thin film hydrophilic polymers. In particular, the high sensitivity of the fluorescence measurement enables one to observe the subtle changes that occur with low amounts of adsorbed water. In medical device manufacturing where thin polymer films are widely used, the ability to observe water adsorption and understand its subtle characteristics will be important for the development of robust manufacturing practices.

Acknowledgment. This work was supported by Science Foundation Ireland under the Research Frontiers Grant 07/RFP/MASF423 to A.G.R.

Supporting Information Available: Further details of the experimental method and fluorescence lifetime data. This material is available free of charge via the Internet at http://pubs.acs.org.

References and Notes

(1) Alarcón, C. D. H.; Pennadam, S.; Alexander, C. *Chem. Soc. Rev.* **2005**, *34*, 276–285.
(2) Fundueanu, G.; Constantin, M.; Ascenzi, P. *Acta Biomater.* **2009**, *5*, 363–373.
(3) Goodwin, A. P.; Mynar, J. L.; Ma, Y.; Fleming, G. R.; Fréchet, J. M. J. *J. Am. Chem. Soc.* **2005**, *127*, 9952–9953.
(4) Kavanagh, C. A.; Gorelova, T. A.; Selezneva, I. T.; Rochev, Y. A.; Dawson, K. A.; Gallagher, W. M.; Gorelov, A. V.; Keenan, A. K. *J. Biomed. Mater. Res., Part B* **2004**, *72*, 25–35.
(5) Kavanagh, C. A.; Rochev, Y. A.; Gallagher, W. M.; Dawson, K. A.; Keenan, A. K. *Pharmacol. Ther.* **2004**, *102*, 1–15.
(6) Kost, J.; Langer, R. *Adv. Drug Delivery Rev.* **2001**, *46*, 125–148.
(7) Miranda, A.; Millán, M.; Caraballo, I. *Chem. Pharm. Bull.* **2006**, *54* (5), 598–602.
(8) Ní Chearúil, F.; Corrigan, O. I. *Int. J. Pharm.* **2009**, *366*, 21–30.
(9) Peppas, N. A.; Huang, Y.; Torres-Lugo, M.; Ward, J. H.; Zhang, J. *Annu. Rev. Biomed. Eng.* **2000**, *2*, 9–29.
(10) Philippova, O. E.; Hourdet, D.; Audebert, R.; Khokhlov, A. R. *Macromolecules* **1997**, *30*, 8278–8285.
(11) Torres-Lugo, M.; Peppas, N. A. *Macromolecules* **1999**, *32*, 6646–6651.
(12) Torres-Lugo, M.; Peppas, N. A. *Biomaterials* **2000**, *21*, 1191–1196.
(13) Wang, G.; Wang, X. *Polym. Bull.* **2002**, *49*, 1–8.
(14) Matsuda, N.; Shimizu, T.; Yamato, M.; Okano, T. *Adv. Mater.* **2007**, *19*, 3089–3099.
(15) Bult, H. *Trends Pharmacol. Sci.* **2000**, *21*, 274–279.
(16) Lewis, A. L.; Tolhurst, L. A.; Stratford, P. W. *Biomaterials* **2002**, *23*, 1697–1766.
(17) Szczupak, B.; Ryder, A. G.; Togashi, D. M.; Rochev, Y. A.; Gorelov, A. V.; Glynn, T. *J. Appl. Spectrosc.* **2009**, *63*, 442–449.
(18) Galaev, I. Y.; Mattiasson, B. *Tibtech* **1999**, *17*, 335–340.
(19) Gil, E. S.; Hudson, S. M. *Prog. Polym. Sci.* **2004**, *29*, 1173–1222.
(20) Aguilar, M. R.; Elvira, C.; Gallardo, A.; Vázquez, B.; Román, J. S. *Top. Tiss. Eng.* **2007**, *3*, 1–27.
(21) Maeda, Y. *Langmuir* **2001**, *17*, 1737–1742.
(22) Schild, H. G. *Prog. Polym. Sci.* **1992**, *17*, 163–249.
(23) de las Heras Alarcón, C.; Pennadam, S.; Alexander, C. *Chem. Soc. Rev.* **2005**, *34*, 276–285.
(24) Cole, M. A.; Voelcker, N. H.; Thissen, H.; Griesser, H. J. *Biomaterials* **2009**, *30*, 1827–1850.
(25) Gras, S. L.; Mahmud, T.; Rosengarten, G.; Mitchell, A.; Kalantar-zadeh, K. *ChemPhysChem* **2007**, *8*, 2036–2050.
(26) Fujishige, S.; Kubota, K.; Ando, I. *J. Phys. Chem.* **1989**, *93*, 3311–3313.
(27) Graziano, G. *Int. J. Biol. Macromol.* **2000**, *27*, 89–97.
(28) Lin, C.-C.; Metters, A. T. *Adv. Drug Delivery Rev.* **2006**, *58*, 1379–1408.
(29) Moran, M. T.; Carroll, W. M.; Selezneva, I.; Gorelov, A.; Rochev, Y. *J. Biomed. Mater. Res., Part A* **2006**, 870–876.
(30) Volpe, C. D.; Cassinelli, C.; Morra, M. *Langmuir* **1998**, *14*, 4650–4656.
(31) Schild, H. G.; Muthukumar, M.; Tirrell, A. *Macromolecules* **1991**, *24*, 948–952.
(32) Bosch, P.; Fernández, A.; Salvador, E. F.; Corrales, T.; Catalina, F.; Peinado, C. *Polymer* **2005**, *46*, 12200–12209.
(33) Ellison, C. J.; Miller, K. E.; Torkelson, J. M. *Polymer* **2004**, *45*, 2623–2632.
(34) Godelle, J. P.; Pearson, R. A.; Santore, M. M. *J. Appl. Polym. Sci.* **2002**, *86*, 2463–2471.
(35) Olmos, D.; López-Morón, R.; González-Benito, J. *Compos. Sci. Technol.* **2006**, *66*, 2758–2768.
(36) Van Der Wel, G. K.; Adan, O. C. G. *Prog. Org. Coat.* **1999**, *37*, 1–14.
(37) Mittal, K. A. *Physiochemical Aspects of Polymer Surfaces*; Plenum: New York, 1983.
(38) La Porte, R. J. *Hydrophilic Polymer Coatings for Medical Devices Structures/ Properties, Development, Manufacture and Applications*; CRC Press: Boca Raton, FL, 1997; Chapter 2.
(39) Kim, M. S.; Paik Sung, C. S. *Fibers Polym.* **2005**, *6*, 127–130.
(40) Szczupak, B.; Ryder, A. G.; Rochev, Y. A.; Klymchenko, A. S.; Gorelov, A.; Glynn, T. J. *Proc. SPIE−Int. Soc. Opt. Eng.* **2005**, *5826*, 1–11.
(41) Bosch, P.; Fernando, C.; Corrales, T.; Peinado, C. *Chem.—Eur. J.* **2005**, *11*, 4314–4325.
(42) Klymchenko, A. S.; Ozturk, T.; Pivovarenko, V. G.; Demchenko, A. P. *Tetrahedron Lett.* **2001**, *42*, 7967–7970.
(43) Klymchenko, A. S.; Ozturk, T.; Demchenko, A. P. *Tetrahedron Lett.* **2002**, *43*, 7079–7082.
(44) Klymchenko, A. S.; Demchenko, A. P. *Langmuir* **2002**, *18*, 5367–5369.
(45) Klymchenko, A. S.; Demchenko, A. P. *Phys. Chem. Chem. Phys.* **2003**, *5*, 461–468.
(46) Klymchenko, A. S.; Duportail, G.; Demchenko, A. P.; Mely, Y. *Biophys. J.* **2004**, *86*, 2929–2941.
(47) Klymchenko, A. S.; Pivovarenko, V. G.; Demchenko, A. P. *J. Phys. Chem. A* **2003**, *107*, 4211–4216.
(48) Klymchenko, A. S.; Pivovarenko, V. G.; Ozturk, T.; Demchenko, A. P. *New J. Chem.* **2003**, *27*, 1336–1343.
(49) Szczupak, B.; Ryder, A. G.; Togashi, D. M.; Rochev, Y. A.; Klymchenko, A. S.; Gorelov, A.; Glynn, T. J. *J. Fluoresc.* **2010**, *20*, 719–731.
(50) Szczupak, B. PhD Thesis, National University of Ireland, Galway, 2009.
(51) Shynkar, V. V.; Mély, Y.; Duportail, G.; Piémont, E.; Klymchenko, A. S.; Demchenko, A. P. *J. Phys. Chem. A* **2003**, *107*, 9522–9529.
(52) Shynkar, V.; Klymchenko, A.; Piemont, E.; Demchenko, A.; Mely, Y. *J. Phys. Chem. A* **2004**, *108*, 8151–8159.
(53) Tamai, Y.; Tanaka, H.; Nakanishi, K. *Macromolecules* **1996**, *29*, 6750–6760.
(54) Tamai, Y.; Tanaka, H.; Nakanishi, K. *Macromolecules* **1996**, *29*, 6761–6769.
(55) Thijs, H. M. L.; Remzi Becer, C.; Guerrero-Sanchez, C.; Fournier, D.; Hoogenboom, R.; Schubert, U. S. *J. Mater. Chem.* **2007**, *17*, 4864–4871.